

Negative differential mobility of weakly driven particles in models of glass formers

Robert L. Jack,^{1,2} David Kelsey,¹ Juan P. Garrahan,³ and David Chandler¹

¹*Department of Chemistry, University of California, Berkeley, CA 94720, USA*

²*Department of Physics, University of Bath, Bath BA2 7AY, UK*

³*School of Physics and Astronomy, University of Nottingham, Nottingham NG7 2RD, UK*

We study the response of probe particles to weak constant driving in kinetically constrained models of glassy systems, and show that the probe's response can be non-monotonic and give rise to negative differential mobility: increasing the applied force can reduce the probe's drift velocity in the force direction. Other significant non-linear effects are also demonstrated, such as the enhancement with increasing force of the probe's fluctuations away from the average path, a phenomenon known in other contexts as giant diffusivity. We show that these results can be explained analytically by a continuous-time random walk approximation where there is decoupling between persistence and exchange times for local displacements of the probe. This decoupling is due to dynamic heterogeneity in the glassy system, which also leads to bimodal distributions of probe particle displacements. We discuss the relevance of our results to experiments.

I. INTRODUCTION

Dynamic heterogeneity manifests complex correlated atomic motions in structural glass forming systems [1]. It is a ubiquitous feature that gives rise to a variety of behaviors peculiar to glassy dynamics. In this paper, we consider phenomena associated with one such behavior – the negative response of a particle's velocity to an applied force. Earlier experiments and computer simulations have studied how particles in glass forming systems respond to external forces [2, 3, 4, 5, 6]. A range of effects have been found, including the appearance of a threshold force [2] and non-linear velocity/force relations [2, 3], the vanishing of the linear response regime at low temperatures [4], the self-organisation of forced particles [5], and negative response to chemical potential gradients [6]. Here, we study the response of a probe particle [7] to a weak external force with numerical simulations and with analytic methods. The numerical work employs kinetically constrained models of glass formers [8, 9]. The analytical work employs a continuous time random walk model [10], specifically the model [11] introduced to treat effects due to decoupling between persistence and exchange processes [7, 12]. While originally constructed in the context of kinetically constrained lattice models, essential features of dynamics that justify this analytical model have been demonstrated in atomistic models of glass formers [13, 14, 15].

Experimental context for our results is shown in Fig. 1: we compare results from one of our model systems with results for a colloidal system near to its glass transition. In order to make contact between model systems and experiments, we plot the probe velocity v and the applied force F in dimensionless units. The velocity is normalised by $v_0 = (D/\sigma)$ where σ is the particle diameter, and D is the diffusion constant of the probe in the absence of the externally applied force. The reduced velocity $|v|/v_0$ is proportional to the 'modified Peclet number' of Ref.[2]. The reduced force is $f = (F\sigma/k_B T)$, where T is the temperature and k_B is Boltzmann's constant. In these units,

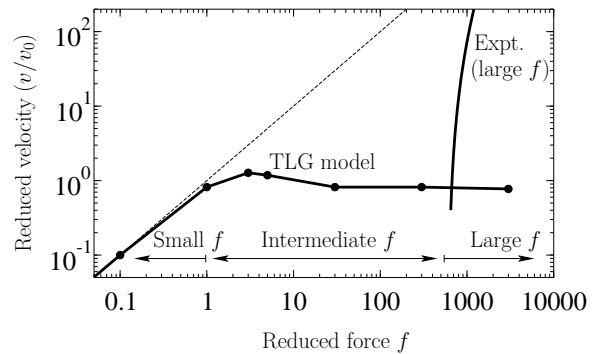


FIG. 1: **Experimental context.** We plot force-velocity relationships in rescaled units, identifying three regimes, as discussed in the main text. The linear response (Einstein) relation, $v = v_0 f$, is represented by the dashed line. At small forces, the predictions of linear response apply. At large forces, the experimental system exhibits a threshold force that represents the limit of applicability of the TLG model. In the intermediate force regime, both the experimental and TLG velocities are much smaller than those predicted by linear response, and the response in the TLG model is non-monotonic. The experimental curve shows the behaviour observed in the colloidal fluid of Ref. [2]: we plot the fitting function $v = v_t [(F/F_t) - 1]^\alpha$ used in [2], with $F_t = 0.6$ pN, $v_t = 2 \times 10^{-1} \mu\text{m s}^{-1}$, and $\alpha = 2.5$. For the experimental data, a reduced force of unity corresponds to $(k_B T/\sigma_{\text{probe}}) \simeq 1$ fN, and $v_0 = (D/\sigma) \simeq 10^{-5} \mu\text{m s}^{-1}$. The data for the TLG model was obtained at filling fraction $\rho = 0.6$.

the linear response formula for the probe velocity is Einstein's relation for small forces, $v = v_0 f$ [16]. Estimating these reduced quantities using data from Refs. [2, 17, 18], we sketch the force-velocity relationship for the colloidal system in Fig. 1, where $v = |v|$ and $f = |f|$.

The experimental data of Ref. [2] has several important features. The most striking is the so-called threshold force, above which the velocity increases rapidly with applied force. On the other hand, for small enough forces, the Einstein relation must apply, although experimental

constraints meant that this regime was not accessible in Ref. [2]. Interestingly, for the experimentally accessible forces below the threshold, the velocity is much smaller than the prediction of linear response: in fact, it was smaller than the experimental resolution limit. We can therefore identify a regime of intermediate force, where the force is much smaller than the threshold, and the response is much smaller than that predicted by the Einstein relation.

According to our theoretical predictions, this regime, which has not yet been investigated experimentally, exhibits new and interesting phenomenology. Figure 1 illustrates our predictions by showing results from our simulations of a kinetically constrained model (details are given below). At small forces, the Einstein relation is obeyed, while the response saturates at larger forces. This saturation represents a non-linear response that is consistent with the small sub-threshold responses observed in Ref. [2]. Our use of kinetically constrained models to describe the colloidal fluid rests on the assumption that glassy behaviour occurs when the motion of particles is constrained by their neighbours. We will see that saturation of the sub-threshold responses is a natural consequence of this assumption. However, it is clear from Fig. 1 that the TLG model does not reflect the experimental observation of a threshold force. Our interpretation of the experimental data is that, as the applied force is increased through the threshold, the force on the probe particle becomes stronger than the constraint forces imposed by its neighbours. As a result, the structure of the colloidal fluid is disrupted by the forced probe. Thus the threshold force represents the limit of applicability of the kinetically constrained model [19]. For this reason, we concentrate in this article on the regime of intermediate forces, where the kinetically constrained model should be applicable. In this regime, we find a surprising effect: increasing the applied force *reduces* the velocity of the pulled particle. This phenomenon and associated results are the focus of this paper.

II. MODELS AND PARTICLE DRIVING PROTOCOLS

We begin by describing the models we use in numerical simulations. Two are “particle” models, in the sense that the material in which the probe moves is described in terms of particles on a lattice with specified dynamical rules. The other is a “field” model in the sense that the material is described in terms of a so-called “mobility” field. The value of that field at a point on the lattice specifies whether or not motion is possible at that point. The specific field model is one of many possibilities, each representing a coarse grained approximation to a particle model [20]. The continuous-time random walk model [11] used later in this paper describes the coupling of the mobility field to particle motion.

A. Particle models

We consider a two-dimensional (i.e., square) version of Kob and Andersen’s (KA) lattice model [21, 22], and the closely related triangular lattice gas (TLG) model of Jäckle and Krönig [23, 24]. These constrained lattice gases are assumed to capture effects of local jamming in a supercooled liquid. They have only excluded volume interactions, so, for a given filling fraction ρ , all allowed configurations are equally likely. They exhibit non-trivial effects of correlated dynamics at filling fractions $\rho \gtrsim 0.5$. Dynamical heterogeneity is manifested as a clustering of mobile particles, and different transport properties decouple from one another (for example, the translation diffusion coefficient does not scale inversely with the structural relaxation time [24]). These effects arise from constraints on the dynamics.

For the KA model [21, 22], specifically the (2,2) variant, particles live on a square lattice, with zero or single occupancy of lattice sites, and a particle may move to adjacent vacant sites only if the particle is adjacent to two vacant sites in both the initial and final sites. Similarly, for Jäckle and Krönig’s TLG model, there is single or zero occupancy on a triangular lattice, and a particle may move to vacant sites only if both of the mutual nearest neighbours of the initial and final sites are vacant. Accordingly, we refer to this model as the (2)-TLG [24]. Its dynamical rules can be motivated on physical grounds by associating hard-cores to the particles, the diameter of which is equal to the lattice spacing, and by insisting that particles move along the lines connecting the points on the lattice. From that picture, it is seen that the dynamical rule is a straightforward steric effect – there is not enough room for a particle to pass to an empty nearest neighbor site unless the two common adjacent sites are also vacant.

In the absence of applied forces, all allowed processes happen with rate γ , which sets the fundamental unit of time. We implement the dynamics using asynchronous Monte Carlo updates.

In order to introduce a force \mathbf{F} on a single “probe” particle, we first consider that particle in an empty lattice. It would correspond to a single colloidal particle alone in a solvent. In the absence of the applied force, this particle has a bare diffusion constant ($\sigma^2\gamma z/2d$) where z is the co-ordination number of the lattice, and we identify the particle diameter σ with the lattice spacing. We denote the force-dependent rates for translational moves of displacement $\Delta\mathbf{R}$ by $W(\Delta\mathbf{R}, \mathbf{F})$. We assume that these rates obey a local form of detailed balance, $W(\Delta\mathbf{R}, \mathbf{F}) = e^{\mathbf{f}\cdot\Delta\mathbf{r}}W(-\Delta\mathbf{R}, \mathbf{F})$, where $\Delta\mathbf{r} = \Delta\mathbf{R}/\sigma$ is a reduced displacement. To ensure that an isolated probe obeys the Einstein relation for all forces, we use the rates

$$W(\Delta\mathbf{R}, \mathbf{F}) = 2\gamma \frac{g(\mathbf{f}\cdot\Delta\mathbf{r})}{1 + \exp(-\mathbf{f}\cdot\Delta\mathbf{r})}, \quad (1)$$

where the dimensionless function $g(E)$ is given by

$$g(E) \equiv E/[2 \tanh(E/2)]. \quad (2)$$

We have $g(0) = 1$, so that $W(\Delta\mathbf{R}, \mathbf{0}) = \gamma$. An alternative choice would be to use Glauber dynamics [$g(E) = 1$ for all E], but in that case, the Einstein relation applies only for small velocities, and there is an unphysical saturation at large forces. This saturation is an artifact of using a lattice to describe continuous space [25]: by using the rates of Equ. (1), we ensure that the velocity of a single particle does not saturate. Hence, the saturating response that we do observe is a physical effect, which appears as the motion of the probe particle becomes increasingly constrained by other particles in the system. We have also checked that while the data presented in this article do depend quantitatively on the choice of $g(E)$, their qualitative features are preserved if we instead use Glauber dynamics. Thus, while there is some arbitrariness in our use of Eq. (1), we are confident that this choice does not affect our main conclusions.

Throughout this article, we consider a single probe in a large system of unforced particles, ignoring the collective behaviour arising from interactions between forced particles [5, 6], and the effect of finite current densities [6]. To enhance statistics, we simulate large systems with a few probe particles in each, and we verify that our results are independent of the number of probes. Due to the underlying lattice, our models are not isotropic, so there is some dependence on the direction of the force compared to the lattice axes (for example, see [3]). However, we find that the results are qualitatively similar for all angles.

B. Mobility field model

We also consider the one-dimensional one spin facilitated Fredrickson-Andersen (FA) model [8, 26, 27]. In this model the local structure is described by a binary variable $n_i \in \{0, 1\}$. Sites with $n_i = 1$ are ‘mobile’, or excited: particles in these regions are able to move; those with $n_i = 0$ are ‘jammed’, so that motion is very unlikely. Sites may change their state only if they are adjacent to a site with $n_i = 1$. In that case they flip from 0 to 1 with rate $c = e^{-\beta}$ and from 1 to 0 with rate unity (this choice sets the unit of time in this model), where β is a dimensionless inverse temperature. The dynamics obey detailed balance, with an energy function $E = \sum_i n_i$, so the equilibrium state has no correlations between sites. This model exhibits effects of non-trivial correlated dynamics for $\beta \gtrsim 1$.

While the relaxation time of the FA model exhibits Arrhenius temperature dependence [9], in $d = 1$ and at low temperature, the model has significant fluctuation effects. These are manifested by stretched exponential relaxation [9] and transport decoupling [7]. Other kinetically constrained models of mobility fields, such as the East model [9, 28] exhibit similar phenomenology in all

dimensions, but the 1d FA model is sufficient to capture the essential physical effects discussed in this article [29].

In Ref. [7], probe particles were coupled to the FA model. Probes were allowed to hop between adjacent sites only when both initial and final sites were mobile. With this choice, the dynamical rules for the n_i do not depend on the positions of the probe particle. While the forced probe is affected by its environment, there is no mechanism for a back-reaction, where the effect of the force feeds back onto the n_i variables. Thus, an excitation in an FA model can pass through this type of probe particle without any knowledge of the probe’s presence. We therefore refer to the probes of Ref. [7] as ‘ghost’ probes.

For particle-based models, including the KCMs introduced above, forced probe particles do have significant effects on their environment. For this reason we introduce an alternative set of rules for probe particles in the FA model, which allow us to model this back-reaction. In particular, since the presence of a probe reduces the available free volume, we imagine that its presence is sufficient to render the site immobile. Thus, we modify the model of Ref. [7] by assuming probes cannot occupy mobile sites. In this case, the probe moves through the system by swapping places with mobility excitations. If the probe position is x , then the allowed moves are

$$(x = i, n_i = 0, n_{i\pm 1} = 1) \rightarrow (x = i \pm 1, n_i = 1, n_{i\pm 1} = 0)$$

Clearly, the dynamics of the FA model itself are now coupled to those of the probes. We therefore refer to these as ‘fully coupled probes’. The rates for attempted moves of both coupled and ghost probes are given by Eq.(1), with $\gamma = 1/2$.

III. FORCE-DEPENDENCE OF THE PROBE VELOCITY

A. Negative differential mobility

The drift velocity of the probe is

$$\mathbf{v} = \lim_{t \rightarrow \infty} t^{-1} \langle \Delta \mathbf{r}_{\text{probe}}(t) \rangle, \quad (3)$$

where $\Delta \mathbf{r}_{\text{probe}}(t)$ is the displacement of the probe in time t , and the average is taken in the presence of the applied force. In Fig. 2(a) we plot this velocity as a function of force in the (2)-TLG and (2,2)-KA models, at densities above their onsets to cooperative dynamics. The linear response (i.e., Einstein) relation is $\mathbf{v} = (D/\sigma)\mathbf{f}$, where D is the zero-force diffusion constant,

$$D = \lim_{t \rightarrow \infty} (2dt)^{-1} \langle |\Delta \mathbf{r}_{\text{probe}}(t)|^2 \rangle_{f=0}. \quad (4)$$

At densities above the onset, $\rho \gtrsim 0.5$, D is much smaller than its bare value ($\sigma^2 \gamma z / 2d$). The striking result of negative response, i.e., negative differential mobility, $dv/df < 0$, is found for $f \gtrsim 2$.

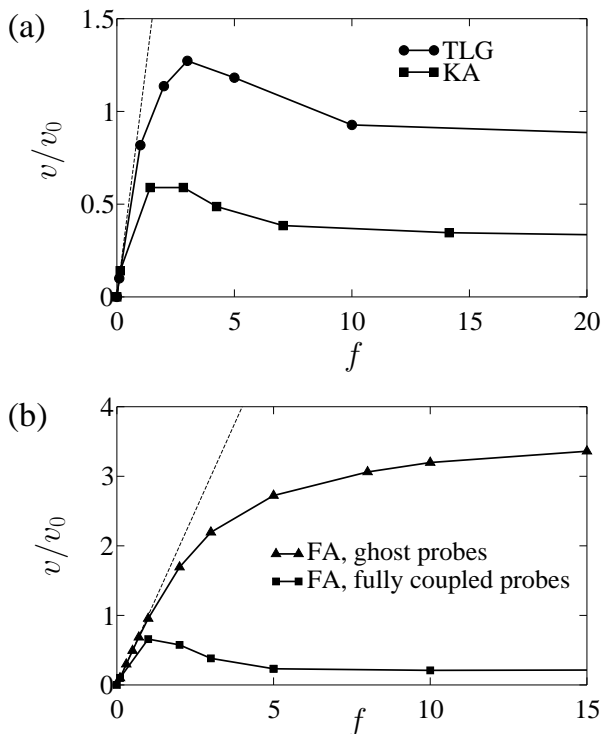


FIG. 2: (a) Non-monotonic velocity-force relationships in particle models, illustrating negative differential mobility. The data for the Jäckle-Krönig TLG model were obtained at filling fraction $\rho = 0.6$, with a force applied along a lattice axis. In the corresponding KA model, the force was applied at 45° to the axes, at filling fraction $\rho = 0.88$. The long time limit in the definition of v necessitates the use of long trajectories (typically $10^4 \tau_\alpha$). (b) Comparison of ghost and fully coupled probes in the FA model in one dimension, at $\beta = 3$. Only the fully coupled probes show a negative differential mobility, indicating that this effect arises from a reaction of the mobility field to the forced probe.

A similar effect is shown in Fig. 2(b) for the fully coupled probes in the FA model. However, negative differential mobility does not occur for the ghost probes. In that case, non-linear effects only lead to a saturation of the drift velocity with force [30]. In Fig. 3, we show how this response depends on the temperature. Keeping the reduced force f fixed, the velocity decreases monotonically as the temperature is reduced. At high temperatures, the dependence on the force is monotonic; negative differential mobility appears below the onset temperature, $\beta \gtrsim 1$. For these temperatures, the linear response (small force) regime is $f \lesssim 1$, and negative differential mobility is observed near $f = 1$, below the onset temperature.

The lack of non-monotonic behavior for ghost particles shown in Fig. 2(b) points to the mechanism for non-monotonic behavior. We use Fig. 4 to illustrate the mechanism. In particular, we show how applying a large force to a probe particle can prevent the movement of neighbouring particles or mobility excitations. For example,

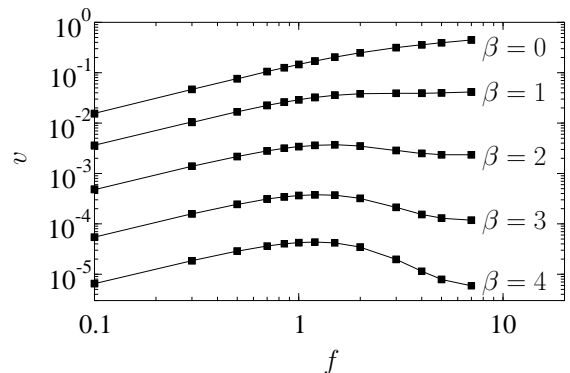


FIG. 3: Data showing the temperature dependence of the velocity-force relationship in the FA model with fully-coupled probes. Non-monotonic response occurs in the low temperature regime $\beta \gtrsim 1$.

Fig. 4(c) shows a configuration in the (2)-TLG for which the probe can make progress in the direction of the force, but only if it first moves backwards, allowing the neighbouring particles to move out of its way. In the FA model, Fig. 4(b), illustrates how a single excitation may allow a single probe to make several steps along the direction of the force [7]. However, this process is suppressed at large forces, since it also involves steps in which the probe moves against the force. At large forces, most encounters between probe and excitation are of the form shown in Fig. 4(a), and the probe makes only one step in each such encounter. In both cases, the forced probe acts to suppress local relaxation, and the force acts to slow down the motion of the probe particle.

The results of Ref. [6] for KA models show a non-monotonic response similar to that of Fig. 2. In that case, all particles attain a finite drift velocity due to force gradients applied to many particles, and large scale density changes result. The effects found in that work are related to those we present here, but in contrast to Ref. [6], the effect we consider arises from forces on a single forced particle that produce no large scale density changes. Non-monotonic response of a drift velocity has also been demonstrated for systems with quenched disorder [31], but the origin of these phenomena is different from those that underlie the results of Ref. [6] and of Fig. 2, where the mechanisms involve the dynamics of the medium.

Finally, we note that the saturation velocity is finite in all of the models that we consider. This is to be contrasted with systems with large numbers of forced particles, in which their velocity may appear to vanish at large forces [6]. For single forced particles, our results suggest that the saturation velocity will be finite as long as the unbiased diffusion constant is finite. [In KCMs with glass transitions at finite densities (or temperatures) [32], all particles are localised in the glass phase: we expect $D = 0$ and $v(f) = 0$ for all f .]

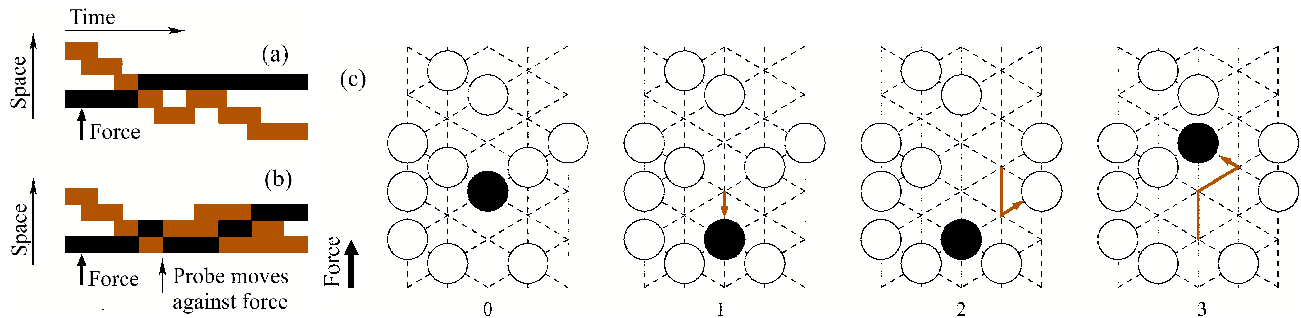


FIG. 4: (Color online) Sample mechanisms for reduced velocity at large forces. (a,b) Sketch of two trajectories in the FA model. Excited sites, $n_i = 1$, are shown in gray (or brown), the trajectory of the probe in black, and time evolves from left to right. (a) A probe moves a single step on encountering an excitation line. (b) An excitation line can facilitate several hops for the probe, increasing its diffusion constant. However, this mechanism requires steps in which the probe moves against the force, so it is suppressed for large forces. (c) A sequence of four configurations that illustrate a co-operative move in the (2)-TLG. The probe (coloured black) responds to the force by eventually moving upwards, but this requires an initial step in which it moves downwards, against the force, to allow the neighbouring particles which are blocking it to move out of the way. Thus the response is again suppressed at large F .

IV. CONTINUOUS TIME RANDOM WALK ANALYSIS

To further elucidate the mechanism for the non-monotonic responses described above, we use a continuous-time random walk (CTRW) analysis [10]. We use the model of [11], which exploits the existence of two separate timescales in glassy systems, corresponding to two different physical processes: exchange and persistence events [11, 12, 14]. Recently, Rubner and Heuer [15] analysed how motion on an underlying energy landscape can result in particle motion that resembles a CTRW. Earlier applications of CTRWs to glassy materials include trapping models such as [33], and mostly focussed on the physical consequences of diverging time scales. In the following, we will assume that all time scales are finite, ensuring that we recover the physical limit of simple diffusion at long times.

A. Theoretical framework

Consider a single probe particle, which makes a series of uncorrelated steps through a fluctuating environment. The force on the probe enters as a bias on the direction of these steps. The probe's environment is dynamically heterogeneous, with space-time permeated with entangled excitation lines [7, 12, 26]. The probe moves only where it is intersected by these lines. In this way, the time between successive steps acquires large fluctuations. We denote the distribution of these times by $\psi(t)$, so that the distribution of time intervals between a randomly selected initial time and the first step made by a particle is [34]

$$p(t) = \frac{\int_t^\infty dt' \psi(t')}{\int_0^\infty dt' \psi(t')}. \quad (5)$$

Following [7, 12], we refer to $\psi(t)$ as the distribution of exchange times and $p(t)$ as the distribution of persistence times. The probability that the particle has made no steps between time 0 and time t , the so-called ‘‘persistence’’ function, is

$$P(t) = \int_t^\infty dt' p(t'). \quad (6)$$

Now, let $G(\mathbf{r}, t)$ be the distribution of the position \mathbf{r} of the probe particle, given that it was at the origin a time t earlier. The number of hops made by the probe in that time is randomly distributed, so $G(\mathbf{r}, t)$ contains a contribution from every possible number of hops. Since successive hops are assumed to be independent, the Fourier-Laplace representation of the sum over these contributions has a closed form: we define $\hat{F}(\mathbf{k}, s) = \int_0^\infty dt \int d^d \mathbf{r} G(\mathbf{r}, t) e^{-i\mathbf{k} \cdot \mathbf{r} - st}$, and arrive at the Montroll-Weiss equation [10, 11]

$$\hat{F}(\mathbf{k}, s) = \hat{P}(s) + \frac{1 - \hat{\psi}(s)}{s} \frac{\Gamma(\mathbf{k})}{1 - \hat{\psi}(s)\Gamma(\mathbf{k})} \hat{p}(s). \quad (7)$$

The functions $\hat{\psi}(s)$, $\hat{P}(s)$ and $\hat{p}(s)$ are the Laplace transforms of $\psi(t)$, $P(t)$ and $p(t)$, respectively. The function $\Gamma(\mathbf{k})$ is the generating function for the statistics of a single random walk step, $\Delta \mathbf{R}$,

$$\Gamma(\mathbf{k}) \equiv \overline{e^{-i\mathbf{k} \cdot \Delta \mathbf{R}}}, \quad (8)$$

where the overbar indicates an average over the possible values of $\Delta \mathbf{R}$. For small wave-vectors, $\Gamma(\mathbf{k}) = 1 - i\sigma \boldsymbol{\delta} \cdot \mathbf{k} - (\sigma^2/2)|\mathbf{k}|^2 + \mathcal{O}(k^3)$, where the invariance of the quadratic term under rotation ensures that unforced diffusion is isotropic, while in the presence of a force there is a non-trivial bias $\boldsymbol{\delta} = \overline{\Delta \mathbf{R}}/\sigma$. The length scale σ would refer to a particle diameter in continuous force models, and here refers to the lattice spacing of our KCMs.

The behaviour of the probe particle at long times is given by the behaviour of $\hat{F}(\mathbf{k}, s)$ at small k and s . We denote the mean exchange and persistence times by τ_x and τ_α respectively (we identify the average persistence time of the probe with the structural relaxation time τ_α of the embedding medium [35]). From (5), we have $\hat{\psi}(s) = 1 - s\tau_x\hat{p}(s)$, and we expand at small s , arriving at $\hat{p}(s) = 1 - s\tau_\alpha + \dots$ and $\hat{\psi}(s) = 1 - s\tau_x + s^2\tau_x\tau_\alpha + \dots$

The drift velocity is then

$$\mathbf{v} = \lim_{s \rightarrow 0} i s^2 \nabla_{\mathbf{k}} \hat{F}(\mathbf{k}, s)|_{k=0} = (\sigma/\tau_x)\boldsymbol{\delta}, \quad (9)$$

where we used $\mathbf{v} = \lim_{t \rightarrow \infty} t^{-1} \int d\mathbf{r} \mathbf{r} G(\mathbf{r}, t)$. Physically, the drift velocity is given by the product of the mean displacement per hop, $\sigma\boldsymbol{\delta}$, and the mean hop frequency, τ_x^{-1} .

Similarly, the asymptotic mean square fluctuation in the probe displacement per unit time is given by

$$\begin{aligned} D(f) &= (2d)^{-1} \lim_{t \rightarrow \infty} t^{-1} [\langle |\mathbf{r}(t)|^2 \rangle - \langle \mathbf{r}(t) \rangle^2] \\ &= (2d)^{-1} \lim_{s \rightarrow 0} [-s^2 \nabla_{\mathbf{k}}^2 \log F(\mathbf{k}, s)|_{k=0} - (|\mathbf{v}|^2/s)] \\ &= (2d\tau_x)^{-1} \{ \sigma^2 + 2|\boldsymbol{\delta}|^2 \sigma^2 [(\tau_\alpha/\tau_x) - 1] \}. \end{aligned} \quad (10)$$

Hence, the unforced diffusion constant is

$$D = D(0) = \frac{\sigma^2}{2d\tau_x}. \quad (11)$$

B. Effect of forcing

From Eq.(9), we see that the probe drift velocity depends on the bias $\boldsymbol{\delta}$ and the mean exchange time τ_x . These quantities depend upon the force. In one dimension, the local form of detailed balance relates the probabilities for hopping to left and right, and we have

$$\delta = \tanh(f/2). \quad (12)$$

This result is independent of the function $g(E)$ in Eq.(1). In $d > 1$, the bias $\boldsymbol{\delta}$ is aligned with the force, as long as diffusion in the unforced case is isotropic. The modulus of $\boldsymbol{\delta}$ increases monotonically with the force, and has a large- f limit $0 < \delta_{\max} \leq 1$.

The dependence of the mean exchange time τ_x on the force manifests the response of the medium on the probe. In the case of a ghost particle, there is no effect so that Eq.(9) gives (in one dimension)

$$[v(f)]_{\text{ghost}} = \frac{\sigma}{\tau_x^{(0)}} \tanh(f/2), \quad (13)$$

where $\tau_x^{(0)}$ denotes the mean exchange time for the medium in the absence of the forced probe particle. This drift velocity follows the Einstein relation for small forces,

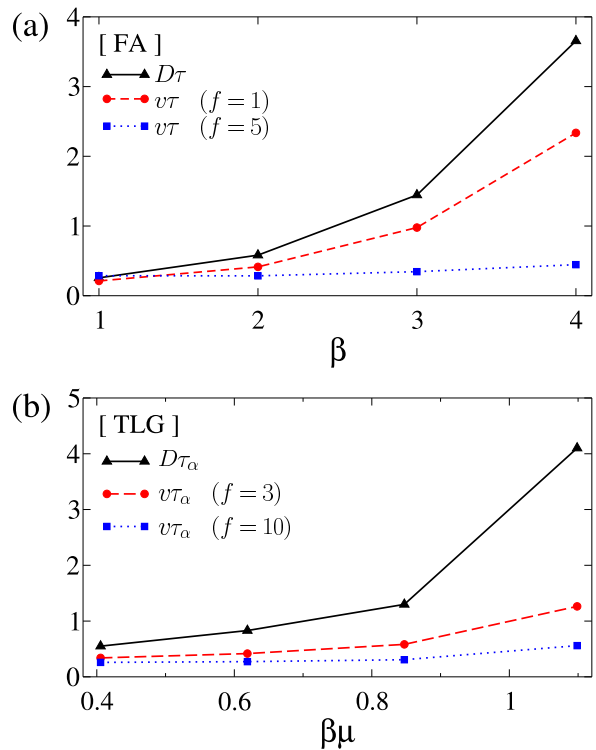


FIG. 5: (Color online) Scaling of the response with temperature and density. We plot rescaled transport coefficients as a function of inverse temperature or chemical potential. (a) FA model: we show the diffusion constant, the velocity at $f = 1$ (close to the maximal response v^*) and the velocity at $f = 5$ (close to the saturation velocity v_{sat}). To investigate the relative scalings of these quantities, we normalise them all by the persistence time τ (which varies by around four orders of magnitude across this temperature range). (b) (2)-TLG, for a range of filling fractions $0.6 \leq \rho \leq 0.75$. We normalise by the structural relaxation time, which increases by a factor of around 300 across this range of density. We define the chemical potential for vacancies to be μ , so that $\rho = (1 + e^{-\beta\mu})^{-1}$ increases from left to right. The maximal and saturation velocities are estimated using $f = 3$ and $f = 10$ respectively.

while for larger forces, it saturates at a limiting value of the order of v_0 . This is illustrated for the $d = 1$ FA model in Fig. 2(b).

More generally, the forced particle does affect its surroundings, and as discussed in Sec. III A and Fig. 4, applying a large force to a probe particle tends to suppress the relaxation of the surrounding medium. In the language of the CTRW, this local slowing down enters as an increase of the mean exchange time.

In fact, Fig. 4(a) indicates that, for large forces in the FA model, the probe typically makes only one step for each excitation that it encounters. For this model, the results of [7, 12] indicate that $\tau_x^{(0)}$ is the typical time between encounters with the same excitation line, while τ_α is the typical time between encounters with different excitation lines. Thus, if the mechanism of Fig 4(a) is

dominating, we expect $\tau_x \approx \tau_\alpha$. However, for small forces, the back reaction of the probe on the medium can be neglected and we expect $\tau_x \approx \tau_x^{(0)}$. To interpolate between these two limits, we combine the rates for the two processes using the simple functional form:

$$\frac{1}{\tau_x} \approx \frac{1 - |\delta|}{\tau_x^{(0)}} + \frac{|\delta|}{\tau_\alpha}. \quad (14)$$

(We choose this form for simplicity, noting that analyses based on it are mostly qualitative, and do not depend on the precise form used.) Using (14) in (9) we then obtain (for $d = 1$),

$$v(f) \approx (2D/\sigma) \tanh(f/2) \left[1 - \frac{\tau_\alpha - \tau_x^{(0)}}{\tau_\alpha} \tanh |f/2| \right]. \quad (15)$$

The velocity v is non-monotonic in f , with a maximum at $f = \mathcal{O}(1)$. This is the non-monotonic behaviour of the drift velocity observed in Fig. 2. The peak value v^* scales with D while the large-force limit of the velocity, v_{sat} , scales with the inverse of τ_α . Thus we expect v^* to scale with D , while $v_{\text{sat}}\tau_\alpha$ depends only weakly on temperature and density. Figure 5(a) shows that the behavior of the fully coupled probe in the FA model is consistent with this analysis. (We have rescaled by the persistence time τ of the excitations n_i , which has the same scaling as the mean persistence time of the probes τ_α [7].) Generalizing (15) to $d > 1$ leads to a similar prediction of non-monotonic response; the scaling of the maximal and saturation velocities is shown in Fig. 5(b), and the qualitative features are again consistent with the CTRW analysis.

C. Force-dependent fluctuations: Giant diffusivity

The analysis also allows us to estimate fluctuations around the average path. In particular, Eqs. (10) and (12) give the force-dependent diffusivity in $d = 1$,

$$D(f) = \frac{\sigma^2}{2\tau_x} \left[1 + 2 \tanh^2(f/2) \left(\frac{\tau_\alpha}{\tau_x} - 1 \right) \right]. \quad (16)$$

Equation (16) shows that increasing the force on the probe particle increases the diffusivity. That is, it leads to larger fluctuations around the average path. For $d > 1$, the functional form of $D(f)$ depends on the relationship between the force f and the bias δ , but the qualitative picture remains the same as in $d = 1$. Moreover, the ratio τ_α/τ_x is related to the Fickian length of [11]:

$$\ell_F \equiv \sqrt{D\tau_\alpha} = \sigma \sqrt{\frac{\tau_\alpha}{2d\tau_x^{(0)}}}. \quad (17)$$

In the deeply supercooled regime this length scale can become large, $\ell_F \gg \sigma$ [11], and the diffusivity $D(f)$ may increase by orders of magnitude as the force is applied.

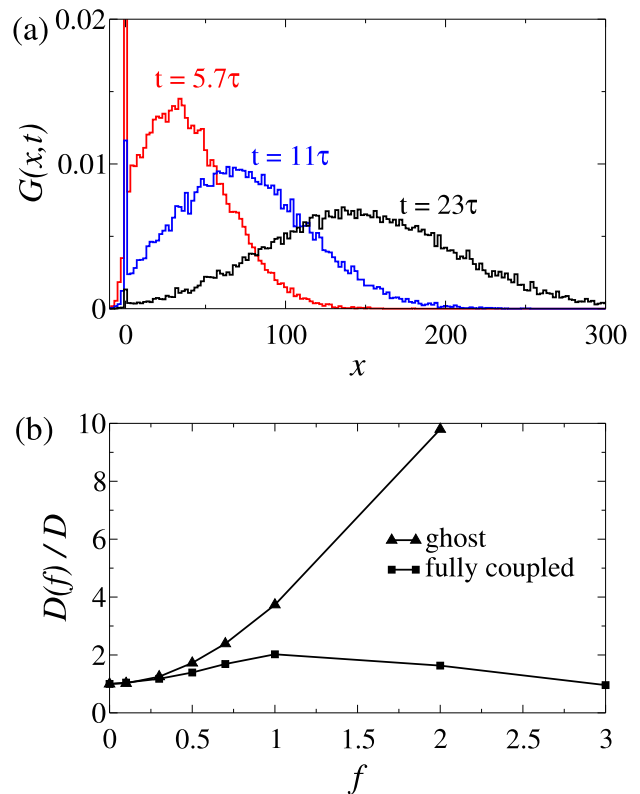


FIG. 6: (Color online) (a) Distribution of the probe displacement parallel to the force, $G(x, t)$, in the FA model at $\beta = 5$ with ‘ghost’ probes, showing a bimodal structure. The force is $f = 0.5$ and the times are given in terms of the persistence time $\tau = 1.15 \times 10^6$ MC sweeps. At the earliest time, the peak at $x = 0$ extends beyond the top of the figure. (b) The force dependent diffusivity $D(f)$ at $\beta = 3$ in the FA model, comparing ghost probes (triangles) with fully coupled probes (squares). The force increases the diffusivity of the ghost probes. For the fully coupled probes, the mechanisms responsible for the negative differential mobility also reduce the diffusivity at large forces.

Fig. 6(b) shows the increase of $D(f)$ with force in the FA model with ‘ghost’ probes. Even at the mildly supercooled conditions shown in the figure, the diffusivity increases by at least an order of magnitude. A significantly smaller increase is found for the case of fully coupled probes. The difference between the two models arises because τ_x increases with increasing force, Eq. (14), so that the contribution of the second term in Eq. (16) is suppressed.

As the relaxation slows in these systems, and fluctuations grow, these non-linear fluctuation effects become important even at small forces. From (16), we can identify the force at which the corrections to the diffusivity become important as $F_{\text{nl}} \approx (k_B T / \ell_F) = (k_B T / \sqrt{D\tau_\alpha})$. Again, the Fickian length grows with decreasing temperature or increasing density, due to the increasing decoupling between diffusion and structural relaxation, and so F_{nl} decreases progressively as the system becomes more

supercooled. A similar criterion was proposed in Ref. [4] for the onset of non-linear effects on probe velocities, $F_{\text{em}} \approx (k_{\text{B}}T/\sqrt{Dt_c})$, where t_c is a relaxation time beyond which certain probability distributions converge to Gaussian forms. The results of that article also indicate a decrease of the threshold force with decreasing temperature.

Finally, the intermittent motion of our forced particle leads to a two-peaked structure in the distribution of the probe displacement, as shown for the FA model in Fig. 6. Similar distributions were observed in the atomistic simulations of Ref. [4] and the experiments of Ref. [37]. They can be interpreted in our dynamical facilitation picture [12, 26] in that the two peaks come from segregation of active populations and inactive populations. Indeed, to a good approximation [11, 36], Eq. (7) gives

$$G(x, t) \approx P(t)\delta(x) + \frac{1 - P(t)}{\sqrt{4\pi tD(f)}} \exp\left\{-\frac{[x - tv(f)]^2}{4tD(f)}\right\}, \quad (18)$$

where x is the displacement in the direction of the force. [Recall that the persistence function $P(t)$ is the fraction of probe particles that have not moved at all between time zero and time t .] This equation for the distribution of probe displacements shows how the decoupling of exchange and persistence times in dynamically heterogeneous materials [12] leads to bimodal distributions such as those of Fig. 6, and hence to the large fluctuations of the sort that in other contexts have been termed “giant diffusivity” [37].

V. OUTLOOK

We have shown in this article that weak forcing of probe particles in KCMs produces surprising non-linear responses such as negative differential mobility and giant diffusivity. The origins of these non-linear effects are the heterogeneity [7, 9] in the dynamics of the probe’s host fluid; the decoupling between local exchange and persistence times [7, 12]; and the consequent intermittency [7, 11] in the motion of the probe. These same mechanisms naturally give rise to transport decoupling in the absence of external forcing (for example, probe diffusion constants and structural relaxation times have different scalings at low temperature [7]). In comparison with other theoretical treatments of transport decoupling [38], ours seems distinguished by the unifying connections it elucidates between the broad distributions of exchange

and persistence times and various observed effects, now including negative response.

All our results are for low-dimensional KCMs. We end with a discussion of how they generalise to three dimensions, and to atomistic or colloidal glass-formers. In explaining the fluctuation phenomena of Sec. IV C, we assumed only that exchange and persistence times decouple from one another. This effect occurs in three-dimensional KCMs in which fluctuations are large (for example, variants of the KA or TLG models). It was also recently demonstrated in three-dimensional atomistic glass-formers [14], and so we expect giant diffusivity to be observed in those systems also. We have discussed how the results of Sec. IV C connect to previous atomistic simulations [4], and experiments would also seem feasible [37].

In addition to decoupling of exchange and persistence times, negative differential mobility depends on a suppression of the local exchange time by the applied force, as discussed in Sec. III A and Sec. IV B. This feature seems to be generic in KCMs, and so we again expect that it would generalise to three-dimensional KA and TLG models. However, such a suppression of the exchange time has not yet been observed in three dimensional atomistic or colloidal systems: we are not aware of experiments that probe the relevant regime (recall Fig. 1). As discussed in Ref. [2], only the large force regime is accessible using that system, since responses below the threshold are smaller than the experimental resolution limits. It seems that experiments with reduced forces $f \simeq 1$ will require the development of new methods. However, searches for giant diffusivity and negative differential mobility, in simulations of glass-formers and in experiments, would provide a further test of the extent to which simple kinetically constrained models can be used to explain and predict the peculiar transport properties of supercooled liquids.

Acknowledgments

In this research, JPG was supported by EPSRC under Grant No. GR/S54074/01. DK was supported initially by the Director, Office of Science, Office of Basic Energy Sciences, Chemical Sciences, Geosciences, and Biosciences Division, U.S. Department of Energy, under Contract No. DE-AC02-05CH11231. RLJ and DC were supported initially by NSF grant CHE-0543158 and later by Office of Naval Research Grant No. N00014-07-1-0689.

[1] For reviews on dynamic heterogeneity see: H. Sillescu, *J. Non-Cryst. Solids* **243**, 81 (1999); M.D. Ediger, *Annu. Rev. Phys. Chem.* **51**, 99 (2000); S.C. Glotzer, *J. Non-Cryst. Solids*, **274**, 342 (2000); R. Richert, *J. Phys. Condens. Matter* **14**, R703 (2002); H. C. Andersen, *Proc. Natl. Acad. Sci. U. S. A.* **102**, 6686 (2005).

[2] P. Habdas *et al.*, *Europhys. Lett.* **67**, 477 (2004).

[3] M. B. Hastings, C. J. Olson Reichhardt, and C. Reichhardt, *Phys. Rev. Lett.* **90**, 098302 (2003); C. J. Reichhardt and C. J. O. Reichhardt, *Phys. Rev. E* **69**, 041405 (2004).

[4] S. R. Williams and D. J. Evans, *Phys. Rev. Lett.* **96**,

- 015701 (2006).
- [5] C. Reichhardt and C. J. O. Reichhardt, Phys. Rev. E **74**, 011403 (2006); *ibid* **75**, 040402 (2007).
- [6] M. Sellitto, Phys. Rev. E **65**, 020101(R) (2002); M. Sellitto, arXiv:0803.2287.
- [7] Y.J. Jung, J. P. Garrahan and D. Chandler, Phys. Rev. E **69**, 061205 (2004).
- [8] G. H. Fredrickson and H. C. Andersen, Phys. Rev. Lett **53**, 1244 (1984).
- [9] F. Ritort and P. Sollich, Adv. Phys **52**, 219 (2003).
- [10] E.W. Montroll and G.H. Weiss, J. Math. Phys. **6**, 167 (1965).
- [11] L. Berthier, D. Chandler and J.P. Garrahan, Europhys. Lett. **69**, 320 (2005); D. Chandler, J.P. Garrahan, R.L. Jack, L. Maibaum, A.C. Pan, Phys. Rev. E **74**, 051501 (2006).
- [12] Y. Jung, J. P. Garrahan and D. Chandler, J. Chem. Phys. **123**, 084509 (2005).
- [13] P. Chaudhuri, L. Berthier and W. Kob, Phys. Rev. Lett. **99**, 060604 (2007).
- [14] L.O. Hedges, L. Maibaum, D. Chandler and J.P. Garrahan, J. Chem. Phys. **127**, 211101 (2007).
- [15] O. Rubner and A. Heuer, arXiv:0802.3516.
- [16] J.-P. Hansen and I. McDonald, *Theory of Simple Liquids*, 2nd ed. (Academic Press, New York, 1986).
- [17] E. R. Weeks and D. A. Weitz, Phys. Rev. Lett. **89**, 095704 (2002).
- [18] When calculating the value v_0 for the experimental data, we use results for the colloid particles of [17] at volume fractions 0.53 – 0.56, since the very small diffusion constants for probe particles are not accurately determined in Ref. [2]. Possible differences in the values of v_0 for probes and colloids should make only small differences on the logarithmic scale used in Fig. 1.
- [19] It would be interesting to investigate the large-force regime by considering KCMs in which constraints can be violated with force-dependent rates. However, while KCMs capture the steric ‘crowding’ effects associated with glassy behavior, details of the interparticle interactions have been coarse-grained away, as have interactions between the particles and the solvent. For these reasons, the development of a lattice model that accurately describes the colloidal system for forces above the threshold is beyond the scope of this paper, and we restrict ourselves to the regimes of small and intermediate force, shown in Fig. 1.
- [20] J.P. Garrahan and D. Chandler, Proc. Natl. Acad. Sci. USA **100**, 9710 (2003).
- [21] W. Kob and H. C. Andersen, Phys. Rev. E **48**, 4364 (1993).
- [22] C. Toninelli, G. Biroli and D. S. Fisher, Phys. Rev. Lett. **92**, 185504 (2004); J. Stat. Phys. **120**, 167 (2005).
- [23] J. Jäckle and A. Krönig, J. Phys.: Condens. Matter **6**, 7633 (1994).
- [24] A.C. Pan, J.P. Garrahan, D. Chandler, Phys. Rev. E **72**, 041106 (2005).
- [25] For diffusion in a continuous medium, the only relevant parameter is the diffusion constant D . In discretising this medium onto a particular lattice with spacing σ , the rate for (unbiased) hops γ is determined by the diffusion constant. If Glauber dynamics are used the maximal probe velocity is $\sigma\gamma \propto (D/\sigma)$. Thus, for a given diffusion constant, the maximal probe velocity is finite in the lattice system, but the saturation disappears in the continuum limit $\sigma \rightarrow 0$. In this sense, the saturation is a lattice artifact.
- [26] J. P. Garrahan and D. Chandler, Phys. Rev. Lett. **89**, 035704 (2002).
- [27] L. Berthier and J.P. Garrahan, Phys. Rev. E **68**, 041201 (2003).
- [28] J. Jäckle and S. Eisinger, Z. Phys. B **84**, 115 (1991).
- [29] We note that the dynamical rules of the East model are not invariant under spatial reflection. However, in the absence of an external field, time reversal symmetry ensures that the probe motion is symmetric in space. It would be interesting to study the interplay between the intrinsic asymmetry of this model and the asymmetric perturbation introduced by the force. In particular, the response of probe particles may depend on the direction of the applied force.
- [30] We have found a similar distinction between ghost and fully coupled probes in other facilitated models, such as Fredrickson and Andersen’s two-spin facilitated model in dimensions two and higher.
- [31] G. A. Cecchi and M. O. Magnasco, Phys. Rev. Lett. **76**, 1968 (1996); R. K. Zia, E. L. Praestgaard and O. G. Mouritsen, Am. J. Phys. **70**, 384 (2002); L. Perondi, J. Phys.: Cond. Matt. **17**, S4165 (2005).
- [32] J. Reiter, F. Mauch and J. Jäckle, Physica A **184**, 458 (1992); C. Toninelli, G. Biroli and D. S. Fisher, Phys. Rev. Lett. **98**, 129602 (2007).
- [33] T. Odagaki and Y. Hiwatari, Phys. Rev. A **41**, 929 (1990); C. Monthus and J.-P. Bouchaud, J. Phys. A **29**, 3873 (1996).
- [34] A proof is given in Ref. [12]. More generally, the fact that the distributions $\psi(t)$ and $p(t)$ are different gives rise to the ‘inspection paradox’. See, for example, W. Feller, *An introduction to probability theory and its applications*, Wiley (New York), 1966.
- [35] While this correspondence is standard in unforced systems [9, 12, 26], the probe persistence time might depend on the applied force. However, while the force-dependence of the exchange time has important consequences (see Sec. IV B), a weak force-dependence of the persistence time has no qualitative effect on our results, so we neglect it.
- [36] The inverse Laplace transform of Eq. (7) gives for the second term of Eq. (18) a convolution between the persistence time distribution and the diffusion propagator. The second term in Eq. (18) is an approximation to that convolution whose long time limit is consistent with Eqs. (9-10), and which captures the crossover from the immobile to the mobile regime. The crossover regime has been considered explicitly in Ref. [13].
- [37] S.H. Lee and D. G. Grier, Phys. Rev. Lett. **96**, 190601 (2006).
- [38] J. A. Hodgdon and F. H. Stillinger, Phys. Rev. E **48**, 207 (1993); G. Tarjus and D. Kivelson, J. Chem. Phys. **103**, 1995 (1995); X. Xia and P. G. Wolynes, J. Phys. Chem. B **105**, 6570 (2001); G. Biroli and J.-P. Bouchaud, J. Phys.: Cond. Matt. **19**, 205101 (2007); K. S. Schweizer, Curr. Opin. Colloid Interface Sci. **6**, 297 (2007).